Geomorphology 460 (2024) 109250

Contents lists available at ScienceDirect

Geomorphology

journal homepage: www.journals.elsevier.com/geomorphology

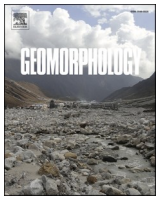

The impact of glacier retreat on Andean high wetlands: Assessing the geochemical transfer and sediment provenance in the proglacial area of Huayna-Potosí (Bolivia)

Ana Navas [a,*], Edson Ramírez [b], Leticia Gaspar [a], Ivan Lizaga [c], Tim Stott [d], Francisco Rojas [b], Borja Latorre [a], Gerd Dercon [e]

[a] Estación Experimental de Aula Dei, Spanish National Research Council (EEAD-CSIC), Avda. Montañana 1005, Zaragoza 50059, Spain
[b] Instituto de Hidráulica e Hidrología, Universidad Mayor de San Andrés, La Paz, Bolivia
[c] Isotope Bioscience Laboratory - ISOFYS, Department of Green Chemistry and Technology, Ghent University, Coupure Links 653, 9000 Ghent, Belgium
[d] School of Biological & Environmental Sciences, Liverpool John Moores University, Byrom Street Campus, Liverpool L3 3AF, UK
[e] Soil and Water Management & Crop Nutrition Laboratory, Joint FAO/IAEA Centre of Nuclear Techniques in Food and Agriculture, Seibersdorf, Austria

ARTICLE INFO

Keywords:
Particulate transfer
Radionuclides
Fingerprinting
FingerPro model
Active landforms
Streambed sediments

ABSTRACT

The accelerated decline of tropical Andean glaciers is affecting the water cycle of mountains in the region. In the Cordillera Real (Bolivia) on the Huayna-Potosí peak (6088 m a.s.l.), the rapid retreat of the Oeste Glacier is exposing new rock outcrops and glacial materials. Changes in the hydrological regime by glacier retreat are likely to modify the supply of sediments and subsequently affect the geochemical transfer of particle-bound elements within proglacial and downstream ecosystems. To address this issue, a sampling campaign in the proglacial area of Huayna-Potosí aimed to identify and collect sediments from the primary active landforms. To characterise elemental transfer and identify sediment provenance using fingerprinting techniques, streambed sediments were collected along the main stream from the glacier tongue at 5002 m a.s.l. to a wetland shallow lake at 4700 m a.s.l.. Geomorphological features control the production of fine particles and the distribution of particle-bound geochemical elements. Complex processes of solubilization, mobilisation, and retention govern the elemental transfer. Significant increases in ^{238}U, as well as some major elements, were observed in the surface lake sediments, while Pb, Cr, and Cu decreased, and ^{137}Cs was not detected. The spatial distribution patterns of geochemical elements and the assessment of the sediment provenance indicate that deglaciation fosters geochemical processes and the elemental transfer dynamics in the wetlands. Moraines and colluvium were found to be the primary contributors to sediment yield (93 %) while the rich organic soils in swamps contributed the least (7 %). The enhanced supply of sediments to the shallow lake in parallel to glacier decline may affect water quality and bring about further changes in the wetlands. Identifying primary sediment sources is essential for water management. Our findings enhance understanding of the compositional characteristics of mobilised sediment and their variations, aiding in more effective resource management to preserve these high-altitude wetlands.

1. Introduction

Most of the world's tropical glaciers are located in the Andes, which hold as much as 99 % of the tropical ice masses, of which 24 % are in Bolivia (da R Ribeiro et al., 2017). The projected temperature increases in the region of around 5 °C to 2100 (Bradley et al., 2006) would lead to the disappearance of small glaciers below 5400 m a.s.l., and the loss of large ice volumes above 6000 m a.s.l. (Réveillet et al., 2015).

Since the Last Glacial Maximum (LGM), the Cordillera Real in Bolivia has undergone intense erosion and carving by glaciers that are currently rapidly receding. As a result, the ensuing landforms have transformed the landscape, with a significant development of glacial and periglacial geomorphic elements. The ongoing glacier retreat has triggered substantial sediment fluxes, and a transition from a glacial to a paraglacial domain as in other world regions (Strzelecki et al., 2017). Moreover, Knight and Harrison (2018) highlights how deglacierizing mountains

* Corresponding author.
E-mail address: anavas@eead.csic.es (A. Navas).

https://doi.org/10.1016/j.geomorph.2024.109250
Received 22 December 2023; Received in revised form 10 May 2024; Accepted 11 May 2024
Available online 20 May 2024

are vulnerable to rapid changes due to high meltwater and sediment fluxes arising from glacier melt.

Within the unstable conditions of paraglacial environments, highly dynamic processes such as runoff, snow and ice melt on slopes and valleys are eroding the glacial and periglacial deposits, thus significantly contributing to the reworking and transport of fine materials across the denuded surfaces. In this sediment cascade, the entrained sediment is subsequently transported towards lower elevations and redistributed to fill depressions, valleys, swales and wetlands. These areas generally act as sediment sinks, but depending on the erosive nature of the prevailing processes, there might also be transport of fine sediments out of the deposition areas.

In the Cordillera Real, the sustainability of high altitude wetlands (bofedales) is under threat due to temperature changes (Lopez-Moreno et al., 2016) and altered rainfall patterns that impact the hydrological cycle of these fragile ecosystems. Groundwater, rain, melting glaciers, and snow contribute water to these high wetlands, which in turn play a key role in storing and supplying water to the Tuni reservoir, the source of water for the city of La Paz. High wetlands act as water reservoirs, refilling during wet seasons and years, and discharging water during dry periods. Wetlands not only facilitate groundwater recharge but also assist in sediment accumulation, contaminant retention, and erosion control (Buytaert et al., 2011). Additionally, their characteristic perennial vegetation serves as forage for the economically significant camelid cattle in the region.

It has been estimated that glaciers contribute around 27 % of the water in the region during the dry season (Soruco et al., 2015). Consequently, glacier recession will specifically impact water resources of the Cordillera Real in Bolivia, posing a threat to wetland conservation (Dangles et al., 2017), as well as endangering water supplies to La Paz, whose population of almost 2 million people has already experienced a water crisis in 2016.

While high wetlands providing essential ecosystem services are currently expanding, the anticipated decrease in glacier melt in the future (Loza Herrera et al., 2015; Dangles et al., 2017) poses a significant threat to the sustainability of wetlands in the arid Puna, which are particularly fragile ecosystems (Vuille et al., 2018). Despite this, Dangles et al. (2017) estimated that there was an increase in wetland surface area in the Cordillera Real between 1984 and 2011, partly due to a higher frequency of extreme events. However, it is also anticipated that glacier runoff will peak at some point this century, which will be followed by a decrease in runoff due to glacier shrinkage (Baraer et al., 2012).

The increased water and sediment discharge will have impacts on ecosystem services in the Andean region (Vuille et al., 2018), as seen in other high mountain regions of Asia (Li et al., 2021), with repercussions for biodiversity and population. Furthermore, the forthcoming effects of climate change over the next decades, particularly on glacierized tropical highlands, demand a deeper understanding of the processes governing sediment transport from source to sink (Fraser, 2012). The imperative for adaptation to ensure ecosystem resilience underscores the need for improved understanding of fine sediment transfer processes and their associated elements, which can have detrimental effects on the quality of natural resources, thereby raising significant environmental concerns (Navas et al., 2020, 2022).

The investigation of proglacial areas of tropical glaciers as regulators of water and sediment fluxes, along with the transport of geochemical elements and nutrients, has received limited attention in high tropical mountains. Studies of the geochemistry of sediment fluxes in paraglacial systems of the central Andes, which are experiencing profound landscape and ecosystem changes, are scarce, while the distinctiveness of the region lies in it being the most diverse and populated high tropical region in the world (Llambí and Cuesta, 2014).

The Cordillera Real at the base of the Huayna-Potosí peak (6088 m a.s.l.) is a unique environment for assessing the transfer of sediments carrying radionuclides, stable elements, and nutrients associated with fine particles along the sediment cascade. In this catchment, the retreat of the glacier has exposed highly reactive rocks and glacial and periglacial materials. These features are pivotal in this paraglacial environment, alongside the expansion of a new lake adjacent to the glacier tongue and the enlargement of wetlands. As part of the IAEA INT5153 project, we conducted a field survey in the proglacial area of Huayna-Potosí during a two-week expedition in May 2017. The objective was to identify the main sediment sources in the area and sample fine materials from moraines, colluvium, and swamps. We also collected fine streambed sediments as representative sediment mixtures along the stream course.

This research aimed to elucidate the transfer of geochemical components associated with the transport of fine sediments across the sediment cascade, from near the glacier tongue (5002 m a.s.l.) to a seasonal lake in the wetlands (4700 m a.s.l.). Additionally, to identify sediment provenance, we applied a state-of-the-art open-source R package-FingerPro model for unmixing sediment mixtures against their sediment sources and quantifying the contributions of different landforms. This would provide insights into any processes of depletion or enrichment from sources to sinks in the wetlands and allow for an evaluation of the origin of the fine particles.

The outcomes of this study would enhance our understanding of the impacts of sediment fluxes in high mountains undergoing rapid deglacierization processes. These findings can assist authorities in meeting water needs amidst glacier decline, benefiting populations, agriculture, and hydroelectric power.

2. Materials and methods

2.1. Study area

In the Eastern Cordillera of the Central Andes, the Cordillera Real (Bolivia) extends over 250 km from southeast to northwest and is around 40 km wide between the Altiplano and the Amazon Basin (Fig. 1). Due to recent glacier recession, glaciated areas in this region are not larger than 150 km^2 and most glaciers are of small size (0.5 km^2) (Dangles et al., 2017; Rabatel et al., 2013). The Last Glacial Maximum (LGM) is dated to 34 Ka at the lowest terminal moraine in Bolivia. The retreat began around 21 Ka to 19 Ka as the climate became warmer and wetter, leading to the formation of lakes. A brief phase of climatic cooling at the end of the Pleistocene lasted 1.3 Ka $\pm$ 70 years. Throughout the Holocene, the dry and warm climate intensified water evaporation, leading to a decrease in the local lake levels (Abott et al., 2000; Thompson et al., 1998). Glacial advancement took place during the Little Ice Age (LIA) occurred in the 17th century. Since then, 10 moraine ridges have been dated in the Cordillera Real (Quimsa Cruz) indicating ongoing glacier retreat up to the present day (Rabatel et al., 2008).

The Huayna-Potosí (16° S, 68° W) is a Triassic intrusion pluton conforming one of the high summits (6088 m a.s.l.) in the core of the Cordillera Real. According to Cordani et al. (2019) the rocks vary between granite and granodiorite composed mainly of quartz, microcline and plagioclase along with biotite and muscovite. In contact with the intrusive batholite, the Palaeozoic Amutara Formation, presenting contact metamorphism of Ordovician sediments (Sempere et al., 2002), is characterized by alternating quartzites up to one metre thick and schists (López Alba, 2014). The soils present in the area are shallow and poorly developed, mainly Leptosols and Regosols, and are affected by cryoturbation in the highest altitudes close to the snow border and covered by shrubs and tussock grasses with decreasing coverage with altitude (Buytaert et al., 2011). The features of rock types, glacial material and soils derived from these parent materials are important for determining the geochemical characteristics of the transported fine sediments.

The regional climate is characterized by two main seasons, wet and dry, that have small temperature variability between seasons though diurnal high contrast between night and day (Buytaert et al., 2010). The

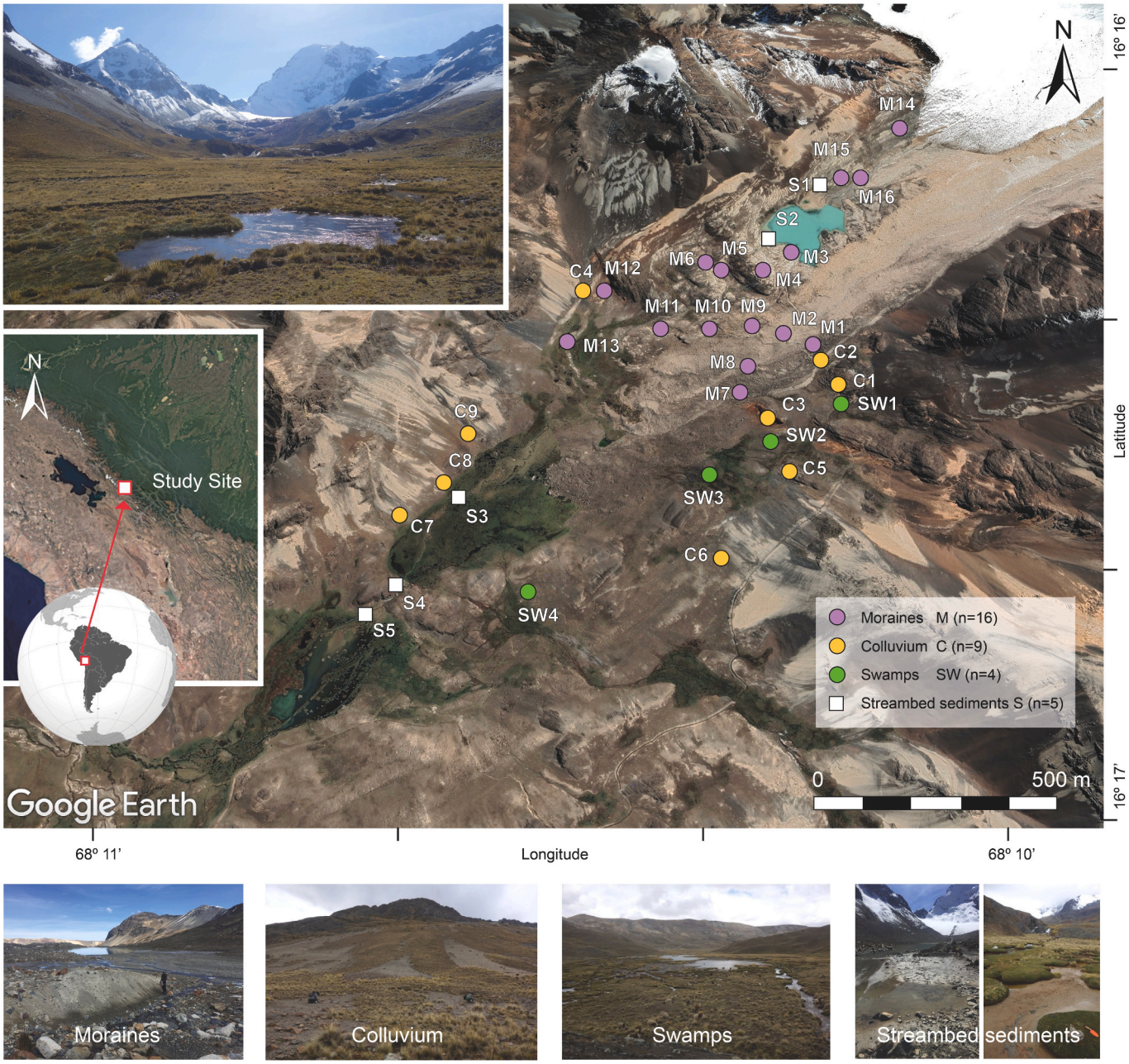

Fig. 1. Location of the study area at the foot of Huayna-Potosí Peak and the Oeste Glacier in the Cordillera Real (Bolivia). Distribution of the sampling points established on the three main landforms: moraines, colluvium and swamps shown in the photographs. Location of the streambed sediments collected downvalley from the headwater by the glacier tongue to the wetlands, ending in the ephemeral wetland lake. The wetlands in the valley and on the slopes appear green in the Google Earth image.

average annual precipitation at the meteorological station of Huayna-Potosí between 2011 and 2015 was 505 mm. Precipitation increases progressively from October, with monthly maximum values ranging from 60 to 136 mm between December and March. During the cooler dry season, which typically occurs in June and July with an average temperature of 0.9 °C, low cloudiness prevails (Dangles et al., 2017). At a multiannual time scale the El Niño Southern Oscillation (ENSO) phases significantly modify the climate patterns with large variability in the precipitation (Garreaud et al., 2003). Among the climate changes recorded in the past century in the region, a decrease in precipitation along with an increase in air temperature is reported (e.g. Vuille et al., 2003, 2008; Lopez-Moreno et al., 2016).

Photogrammetric restitutions from an aerial flight conducted in 1975 by the Bolivian Air Force (FAB) and high-resolution panchromatic images of 2021 from the Brazilian satellite CBERS-4 A following procedures by Ramírez et al. (2001) and da R Ribeiro et al. (2013) were carried out to assess the dynamics of the glacier retreat (Fig. 1 Supplementary materials).

In the proglacial area of the Huayna-Potosí there are eight permanent wetlands, four along the valley and another four on the slopes (Fig. 1) that are affected by the rapid retreat of the glacier. The high altitude wetlands occupy the floor of the glacial U-shaped valley downstream to Tuni village, the largest distance reached by the ice masses here during the LGM. The flat topography of the valley favours the formation of shallow depressions that are fully or partially filled with water, especially during the wet season, and are enclosed within the moraine arcs close to the glacier tongue, but there are also slope wetlands that are fed by permanent water springs. Wetlands have hydromorphic conditions,

high levels of soil organic carbon and nitrogen, and high infiltration rates, leading to a high water storage capacity that promotes subsurface runoff (Liberman, 2021). The typical vegetation cover of the wetlands includes cushion plants of the *Juncacea* and *Cyperaceeas* families with abundance of *Distichia muscoides* in the hummock communities and *Ranunculus uniflorus* among the aquatic macrophytes.

2.2. Sampling design

To assess the geochemical characteristics of the landforms that could potentially deliver fine sediments into the hydrological system and the associated geochemical transfer in the valley floor wetlands a field survey was conducted (Fig. 2). Three main geomorphological units were identified: moraines exposed after the glacier retreat (M), colluvium (C), which are steep deposits covering the slopes of the deglaciated peaks surrounding the valley floor, and swamps (SW) located on the slopes, where spring water flows down to the valley floor, holding very rich organic soils.

The sampling sites were distributed in the three study units according to the space occupied by the landforms in the proglacial area. Surface sediment samples (0–2 cm depth) were collected at sites that had good connectivity with the hydrological system to ensure the export of the fine material to the wetlands. Each sample was composed of five subsamples that, depending on the homogeneity of the site, were separated by around 10 to 20 m.

The moraines are composed of loose heterometric glacial material from the granitic batholith of the Huayna-Potosí and the Ordovician rock outcrops of the metamorphic contact aureole, conforming to the adjacent relief around the glacial valley. A total of 16 moraine samples were collected along the succession of moraine arcs. In the colluvial mantles covering steep slopes, nine sampling sites were established to collect the fine material resulting from the physical weathering of the quartzite and phyllite rock outcrops. In the swamps around the main slope springs, a total of 4 composite samples were collected in the streambanks of the shallow soils.

To assess the geochemical transfer in the wetlands, fine streambed sediments were collected along the main water course flowing from the glacier in the proximity of the tongue of the Oeste Glacier at 5002 m a.s.l., (S1) before entering the new expanding lake, and at the outlet of the lake (S2) where the river is incising the moraine. Another three sediment mixtures (S3, S4 and S5) were collected down the valley in the small canals formed between cushion plants in the wetlands. The final point, S5, also used for quantifying the sediment provenance, was located at 4700 m a.s.l. after the river dissected the rock outcrops ending in the larger wetland that forms a shallow lake in the wet season (Fig. 1).

The collection of sediment samples was undertaken in the dry season and rainfall did not occur during the field campaign. Therefore, the streams were not carrying suspended sediments and discharge was mainly from the melting of glacier ice and water stored in the wetlands.

2.3. Sample preparation and analyses

The preparation of the sediment samples for analyses follow established protocols. Samples were dried, ground, homogenised and sieved to ≤63 μm. This size fraction has been selected based on the granulometric distribution of the collected samples but also because it is the fraction most widely used to assess the geochemical composition of particulate transport in a variety of environments (Owens et al., 2016; Collins et al., 2020; Navas et al., 2022).

The pH and electrical conductivity (EC dS m^{-1}) were analysed by standard methods. The analyses of the grain size distribution (sand, silt and clay) in the ≤63 μm fraction were performed by laser Coulter

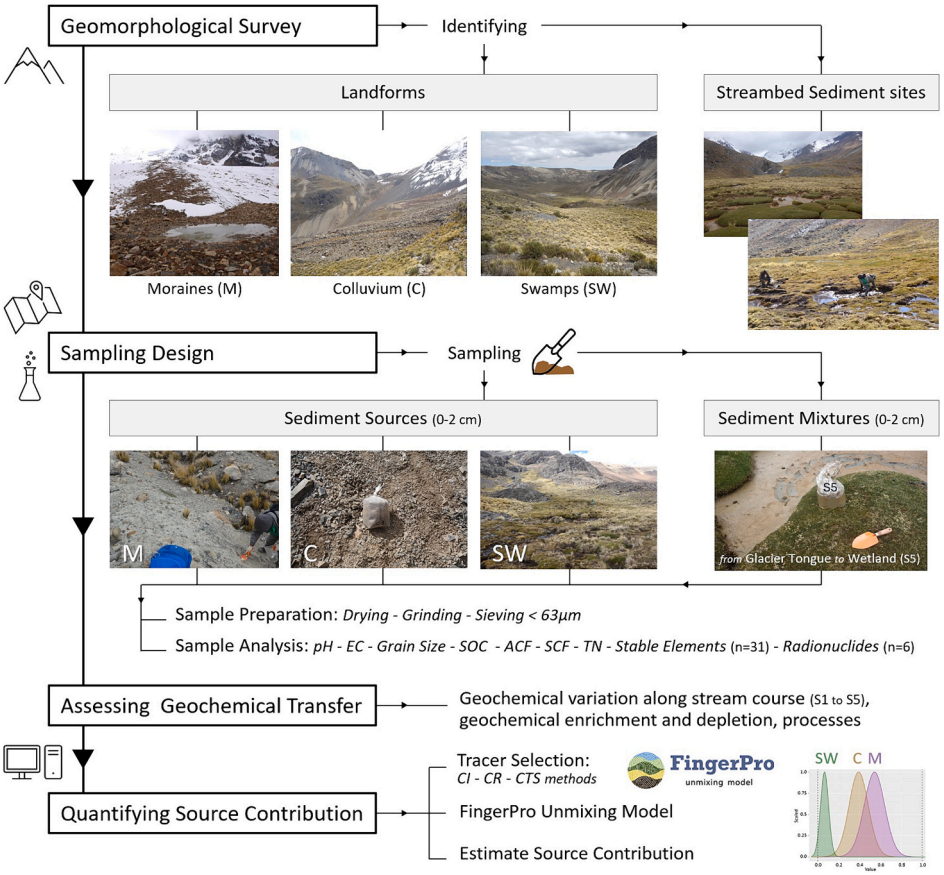

Fig. 2. Flowchart of the research procedure and steps of the study in sequential order.

Counter after eliminating the organic matter, disaggregating with sodium hexametaphosphate, stirring for 2 h and applying ultrasound. The organic carbon content (SOC, %) was measured with the dry combustion method at 550 °C using a LECO, RC-612 multiphase carbon analyser. The active and stable carbon fractions were analysed using the same equipment, with temperatures stepped at 350 °C to oxidize the active (ACF) and at 550 °C for stable carbon (SCF) (Quijano et al., 2016). The total nitrogen content (TN) was measured using a LECO CN TruSpec nitrogen analyser by determining the NOx gas evolved after combustion at 950 °C by a thermal conductivity detector.

A total of 37 geochemical components were analysed: of which 31 stable elements (Al, As, Be, Bi, B, Ca, Cd, Co, Cr, Cu, Fe, K, La, Li, Mg, Mn, Mo, Na, Ni, Pb, P, Rb, Sb, Se, Si, S, Sr, Ti, Tl, V and Zn) and 6 radionuclides (fallout radionuclides, FRNs) ^{137}Cs, ^{210}Pb$_{ex}$, and 4 environmental radionuclides (ERNs) ^{226}Ra, ^{238}U, ^{232}Th and ^{40}K). The elemental contents (mg kg^{-1}) were analysed by ICP-AES after total acid digestion with HF (48 %), HNO_3 and H_2O_2 followed by a second extraction with HNO_3, HCl in a microwave oven (Navas and Machín, 2002).

Analyses of radionuclides (Bq kg^{-1}) were performed at the gamma lab of the Experimental Station of Aula-Dei (EEAD-CSIC), using a high resolution, low background, hyperpure germanium coaxial gamma detector (Canberra Xtra, 50 % efficiency, 1.9 keV resolution). Standard certified samples in the same geometry as the measured samples were used for calibration (Navas et al., 2017). The activity of ^{137}Cs was determined from the 661.6 keV photopeak; ^{210}Pb was measured at 46.5 keV; ^{226}Ra was determined from the 351.9 keV line of ^{214}Pb, a short-lived daughter of ^{226}Ra, after equilibrium was reached. Unsupported ^{210}Pb$_{ex}$ activity was estimated by subtracting ^{226}Ra from total ^{210}Pb; ^{238}U was determined from the 63-keV line of ^{234}Th; ^{232}Th was estimated using the 911-keV photopeak of ^{228}Ac and ^{40}K was determined from the 1461 keV photopeak. Counting times of 86,400 s provided an analytical precision of about ±3–10 % at the 95 % level of confidence for the radionuclide activities (Bq kg^{-1} dry soil).

2.4. Quantifying the sediment provenance

Fingerprinting methods have significantly advanced in the past two decades. Various models, including Bayesian and deterministic models, have been developed to estimate the contribution of sediment sources to target sediment mixtures through different approaches (e.g. Collins and Walling, 2002; Martínez-Carreras et al., 2010; Blake et al., 2018; Evrard et al., 2020). Greater complexity arises from the use of an expanding array of fingerprints (e.g. Owens et al., 2016; Lizaga et al., 2024).

For identifying the sediment provenance and quantifying the percentage contribution of each of the three main sources to the streambed sediments collected at the entrance of the final wetland in the ephemeral lake (S5), we applied a state-of-the-art open-source R package-FingerPro model (Lizaga et al., 2020a) (Fig. 2).

The relative contribution of each potential sediment source is determined using a standard linear multivariate mixing model:

$$\sum_{j=1}^{m} a_{i,j} \bullet \omega_j = b_i$$

which satisfies:

$$\sum_{j=1}^{m} \omega_j = 1$$

$$0 \leq \omega_j \leq 1$$

where b_i is the tracer property i ($i = 1$ to n) of the sediment mixture, $a_{i,j}$ represents the tracer property i in the source type j ($j = 1$ to m), ω_j is the unknown relative contribution of the source type j, m represents the number of potential sediment sources and n is the number of tracer properties selected.

The model sensitivity was successfully tested using geochemical fingerprints with artificial mixtures (Gaspar et al., 2019a). The appropriate selection of tracers that better discriminate the sources is approached by using firstly, the conservativeness index (CI) and the consensus ranking (CR) methods (Lizaga et al., 2020b) to identify tracers exhibiting apparent non-conservative and non-consensual behaviour. The CI is a non-parametric test that analyses tracer conservativeness using mixture and source data to create an index that is a more sophisticated version of the range test. The CR is a scoring function that involves multiple random debates between tracers, with the tracers preventing consensus being discarded. It is important to note that different mixtures, subjected to varying physical and chemical processes, will result in different mixture values and, consequently, different optimal tracer selections (Gaspar et al., 2019b; Lizaga et al., 2020b).

Finally, the consistent tracer selection (CTS) method (Latorre et al., 2021) as a more advanced discriminant function analysis, identifies the most discriminant tracers while also examining their mathematical properties to ensure consistency in over-determined datasets that otherwise could introduce bias in all type of models (e.g., three sources and three or more tracers). For the study dataset commencing with the optimal pair of tracers characterized by the lowest dispersion and high consensus (CR > 90), we progressively incorporated tracers from the dataset that maintained solution consistency ($\varepsilon < 0.066$). Once the tracers are selected, the unmixing model provides the source apportionment solutions that are expressed by the mean and standard deviation calculated from the model results.

3. Results

3.1. Geochemical characteristics of the landforms and streambed sediment

The succession of moraines at the foot of the Huayna-Potosí conform to a hilly smoothed relief that holds a sequence of relatively recent wetlands that developed subsequent to the recession of the glacier after the Little Ice Age (LIA). The glacial materials exhibited considerable heterogeneity, comprising angular to sub-angular blocks, cobbles, pebbles, and gravels derived from an array of granitic and metamorphic rock types. These components are embedded within the assayed silty matrix (Table 1). The periglacial colluvial materials displayed similar heterogeneity, comprising angular blocks, cobbles, pebbles, and a silty matrix.

The silt fraction was the most abundant, particularly pronounced in colluvium and swamps compared to moraines that had a significantly higher sand content. Nevertheless, there were no significant differences in clay content, although colluvium had the highest levels. The acidic pH varied little in moraines and colluvium but significant differences were found in swamps, where the mean pH value was 6. Very low salinity was recorded in moraines compared to swamps, where average EC was 0.5 dSm^{-1}, while salts were not detected in colluvium. Calcium carbonate was absent in all the study samples.

The content of organic carbon varied widely, ranging from undetectable levels in three moraine points near the glacier tongue (M14, M15, M16), to low percentages in other moraines and colluvium samples (means: 0.4 and 1.1 %, respectively). Notably, swamps had very high organic carbon content. The stable carbon fraction was less prevalent, showing significant differences in moraines compared to colluvium and swamps. In contrast, the active carbon fraction was more abundant, especially in swamps, reaching up to 24.8 %. Nitrogen content in swamps was also notably higher, up to tenfold compared to moraines, which had the lowest nitrogen contents near the glacier tongue. However, colluvium had slightly higher nitrogen content, significantly different from both moraines near the glacier and swamps, with levels approximately five times lower than those observed in swamps.

Table 1
Characteristics of main physico-chemical properties (mean, sd) assayed in the fine material of the landforms. Anova test: Asterisks indicate significant differences among landforms ($p \leq 0.05$). Fisher's *Least Significant Differences* (LSD) test: Different letters indicate significant differences between each landform ($p \leq 0.05$).

		Moraines ($n = 16$)		Colluvium ($n = 9$)		Swamps ($n = 4$)		Anova test	Fisher's LSD test		
		Mean	SD	Mean	SD	Mean	SD	*p* value	M	C	SW
Clay	%	8.2	2.3	10.1	3.2	8.5	2.2	0.212	a	a	a
Silt	%	68.7	3.5	71.5	1.5	73.8	5.3	0.017	a	ab	b
Sand	%	23.1	4.9	18.4	2.8	17.7	5.2	0.019	b	a	a
SOC	%	0.4	0.5	1.1	0.6	22.2	2.3	0.000	a	a	b
ACF	%	0.3	0.3	0.7	0.4	21.6	2.6	0.000	a	a	b
SCF	%	0.1	0.1	0.4	0.2	0.6	0.4	0.000	a	b	c
TN	%	0.1	0.0	0.2	0.1	1.1	0.1	0.000	a	b	c
pH		5.2	0.8	5.1	0.6	6.0	0.2	0.098	a	a	b
EC	dS m^{-1}	0.1	0.0	0.0	0.0	0.5	0.1	0.000	a	a	b

sd: *standard deviation.*

In the proglacial area, the most abundant stable elements were Fe and Al, followed by Si, K, Na, Ti, Mg, and Ca, then P, B, Mn, S, Tl and As (Table 2). Minor elements in descending order were Zn, V, Sr, Li, Cr, Pb, Cu, Rb, Bi, Ni, and Co. As trace elements, La, Be, Cd, Mo, Sb, while Se was mostly below detection limits. Similar abundance patterns were observed in the streambed sediments, except for enhancements of Mg, B, S, As, Zn, and Rb. Additionally, Pb and La contents nearly doubled those in the landforms, while depletion only affected Ti, Tl, and Mo. The lowest radionuclide activities were observed for ^{137}Cs, while the highest were for ^{40}K. The levels of FRN were significantly lower in the streambed sediments. However, the mass-specific activities of the environmental radionuclides were similar in the landforms and the streambed sediments. In contrast, the ^{238}U activities in the streambed sediments were twice those of the sources (Table 2).

Table 2
Basic statistics for the mass activity of fallout and environmental radionuclides and stable elements content assayed in the landforms and the streambed sediments.

	Landforms ($n = 29$)			Streambed sediments ($n = 5$)		
	Mean	SD	CV %	Mean	SD	CV %
Radionuclides Bq kg^{-1}						
^{137}Cs	2.1	1.9	87.0	0.3	0.5	183.3
$^{210}Pb_{ex}$	105.1	53.1	50.5	42.7	7.4	17.3
^{226}Ra	54.8	18.2	33.2	61.3	2.4	3.9
^{232}Th	69.9	18.9	27.1	66.8	9.4	14.0
^{238}U	96.8	20.3	20.9	184.4	52.2	28.3
^{40}K	841.5	204.3	24.3	847.0	130.5	15.4
Stable elements mg kg^{-1}						
Fe	39,929.0	15,094.3	37.8	34,686.0	7189.7	20.7
Al	34,473.8	8713.3	25.3	36,432.0	5170.3	14.2
Si	20,478.1	7841.9	38.3	21,062.0	875.5	4.2
K	17,344.3	4494.9	25.9	21,672.0	2154.9	9.9
Na	10,008.3	4160.3	41.6	12,512.0	999.5	8.0
Ti	6205.6	1894.5	30.5	6140.0	424.5	6.9
Ca	3843.2	2508.7	65.3	4163.2	650.9	15.6
Mg	3296.4	1589.4	48.2	5202.8	900.9	17.3
P	1230.2	277.1	22.5	1425.8	75.9	5.3
B	1135.4	472.6	41.6	1557.6	90.5	5.8
Mn	845.8	665.9	78.7	640.3	91.2	14.2
S	666.9	872.1	130.8	876.8	1169.9	133.4
Tl	223.2	238.2	106.7	61.3	125.9	205.2
As	142.6	130.7	91.7	247.6	97.4	39.4
Zn	88.7	28.2	31.8	162.8	24.5	15.1
V	72.0	20.4	28.4	68.9	14.3	20.7
Sr	63.5	23.2	36.5	76.3	6.6	8.6
Li	63.9	21.9	34.2	72.0	15.5	21.5
Cr	59.8	14.6	24.4	62.0	11.4	18.4
Pb	57.1	41.2	72.2	102.5	34.8	33.9
Cu	45.8	55.2	120.5	42.4	9.4	22.3
Rb	27.7	13.0	47.0	42.2	5.4	12.8
Bi	26.3	7.4	28.3	26.7	3.8	14.1
Ni	22.9	8.4	36.8	34.1	7.4	21.6
Co	20.2	7.2	35.7	20.5	2.8	13.8
La	3.6	3.2	90.7	6.5	2.1	31.8
Be	2.8	0.8	27.4	3.2	0.6	20.2
Cd	1.4	0.8	59.8	1.7	0.6	31.6
Mo	1.5	0.8	51.1	1.4	0.3	21.9
Sb	1.1	0.7	62.5	0.2	0.4	223.6
Se	0.3	0.5	154.5	0.6	1.0	169.2

sd *standard deviation*; CV *coefficient of variation.*

Significant differences ($p \leq 0.05$ %) were found in the contents of most stable elements (except for Fe, P, B, Tl, Zn, Sr, Li, Cr, Bi, Cd and Se) among the three sediment sources: moraines, colluvium and swamps. While the latter were most variable, moraines and colluvium shared more similarities in stable element contents (Table 3). This trend was also evident in the radionuclide activities, with ^{238}U and ^{137}Cs being similar in colluvium and swamps, while swamps showed the most differentiation in the remaining radionuclides. Thus, FRN activities were highest in swamps, while the opposite was recorded for ERNs.

Based on the general properties, stable elements and radionuclide values a clear discrimination among the landforms was evident in the scatter plot of the Linear Discriminant Analysis (LDA) (Fig. 3). The results of the principal component analyses using 37 variables (5 properties (clay, silt, sand, SOC and TN), 26 stable elements and 6 radionuclides) displayed three main principal components explaining 67.1 % of the total variance. The scatter plot of the first three principal components (Fig. 3) illustrated these relationships. Component 1 (37.7 % of total variance) highlighted the association of nutrients (SOC and Nitrogen) with fallout radionuclides and certain elements like Fe, Mn, S and Mo, prevalent in swamps, however nutrients were inversely associated with lithogenic radionuclides and most major elements, while conversely sand showed direct correlation with lithogenic radionuclides and most stable elements. In component 2 (17.1 % of total variance), sand was linked with ^{238}U, Ca, Na, Mg, Sr and Rb, while clay correlated with ^{232}Th and ^{40}K and minor elements. In contrast, component 3 (12.3 % of total variance) showed associations between clay and fallout radionuclides, as well as with major elements.

The spatial distribution of radionuclides and stable elements in the proglacial area showed distinct features (Fig. 2 Supplementary Materials). While fallout radionuclides were very low in moraines near the glacier tongue for $^{210}Pb_{ex}$, while ^{137}Cs being absent, they reached their highest levels in swamps and certain colluvium sites adjacent to metamorphic outcrops on the east side. Opposite, the contents of lithogenic radionuclides were very low in swamps but abundant in moraines beneath the expanding lake, particularly for ^{226}Ra, ^{232}Th and ^{40}K. Similarly, ^{238}U contents were low in swamps and recently exposed moraines near the glacier tongue. Major element abundance (Al, Si, K, Na, Ti, Mg and P) was mainly associated with moraines, with lesser contents in certain colluvium sites except for those on the west side, while lower contents appeared in swamps. Although, Ca was more abundant in moraines, high levels were also found in swamps. However, Fe had low contents in moraines but was concentrated in some swamps and colluvium sites on the east side. High S levels were observed in swamps and one recently exposed moraine near the glacier tongue. Additionally, Mn also predominated in swamps, while B was highest

Table 3
Mass activity of fallout and environmental radionuclides and stable elements contents (mean, sd) assayed in the landforms. Kruskal Wallis test: Asterisk indicate significant differences of median values among landforms ($p \leq 0.05$). Fisher's *Least Significant Differences* (LSD) test: Different letters indicate significant differences between each landform.

	Moraines (n = 16)		Colluvium (n = 9)		Swamps (n = 4)		KW test		Fisher's LSD test		
	Mean	SD	Mean	SD	Mean	SD	*P value*		M	C	SW
Radionuclides Bq kg^{-1}											
^{137}Cs	1.3	1.5	2.6	1.8	4.3	0.8	0.010	*	a	ab	b
^{210}Pb$_{ex}$	87.8	46.7	104.5	37.3	175.9	58.3	0.045	*	a	ab	b
^{226}Ra	62.9	14.6	55.4	4.5	20.8	7.8	0.005	*	b	b	a
^{232}Th	74.7	14.8	77.2	7.9	34.0	9.3	0.006	*	b	b	a
^{238}U	103.3	20.8	85.8	10.9	95.6	27.6	0.084		b	a	ab
^{40}K	918.9	107.4	892.2	97.3	417.5	165.1	0.005	*	b	b	a
Stable elements mg kg^{-1}											
Fe	35,158.8	6860.4	40,906.7	18,827.6	56,810.0	21,016.8	0.244		a	ab	b
Al	40,065.6	4952.3	30,484.4	6435.4	21,082.5	4682.5	0.000	*	c	b	a
Si	23,867.3	6623.1	19,335.6	6845.6	9492.3	1887.6	0.008	*	b	b	a
K	19,716.9	2669.1	16,971.1	2100.4	8693.5	3311.6	0.000	*	c	b	a
Na	12,189.6	3947.1	8481.8	2141.3	4718.3	1316.5	0.001	*	b	a	a
Ti	7145.6	1103.8	6262.2	675.7	2317.9	1146.7	0.001	*	c	b	a
Ca	4295.2	2395.9	1714.4	802.6	6825.0	1334.4	0.002	*	b	a	c
Mg	4421.9	1108.4	1943.6	913.5	1838.3	358.5	0.000	*	b	a	a
P	1308.4	146.3	1202.0	376.1	980.6	338.0	0.234		b	ab	a
B	1184.8	467.6	1207.4	523.4	776.0	246.1	0.182		a	a	a
Mn	530.1	94.5	902.3	653.9	1981.5	832.7	0.008	*	a	a	b
S	407.3	509.6	316.9	245.4	2493.0	683.1	0.007	*	a	a	b
Tl	184.4	132.2	151.6	194.6	539.2	429.9	0.086		a	a	b
As	152.1	117.8	71.2	37.4	265.4	224.7	0.029	*	ab	a	b
Zn	87.9	28.3	93.8	29.5	80.1	30.3	0.511		a	a	a
V	66.9	10.3	94.3	12.3	42.6	14.0	0.000	*	b	c	a
Sr	69.7	21.1	49.8	20.6	69.6	29.1	0.120		b	a	ab
Li	69.4	24.2	64.4	9.4	40.8	20.7	0.113		b	ab	a
Cr	56.4	11.9	65.3	14.7	61.3	23.5	0.297		a	a	a
Pb	72.2	47.1	44.9	24.3	24.0	5.4	0.001	*	b	ab	a
Cu	33.2	19.0	79.9	89.6	19.8	6.7	0.002	*	a	b	ab
Rb	36.6	10.3	18.2	5.9	13.9	4.2	0.000	*	b	a	a
Bi	23.7	3.5	28.7	8.5	31.8	12.9	0.179		a	ab	b
Ni	20.5	4.9	30.7	8.8	14.9	6.0	0.001	*	a	b	a
Co	16.9	4.4	26.6	8.7	19.2	2.4	0.013	*	a	b	a
La	5.6	2.8	0.3	0.6	3.0	1.7	0.000	*	b	a	ab
Be	3.0	0.7	2.8	0.7	1.7	0.3	0.011	*	b	b	a
Cd	1.2	0.4	1.2	0.7	2.3	1.6	0.423		a	a	b
Mo	1.0	0.3	1.9	0.7	2.3	0.9	0.000	*	a	b	b
Sb	1.1	0.5	1.5	0.7	0.2	0.3	0.005	*	b	b	a
Se	0.2	0.3	0.6	0.7	0.2	0.4	0.269		a	a	a

sd *standard deviation.*

near the glacier tongue and in colluvium of the east side, as well as moraines on the west side.

Concerning minor elements, Zn predominated also on the east side and in recent moraines near the glacier tongue, but less abundant in some swamp points. However, As abundance was highest in headwater moraines and swamps that also contained high levels of Tl. Strontium and Li predominated in the moraines below the expanding lake, while V content was higher in most colluvium points. The abundance of Cr, Ni, Bi and Cu showed no clear spatial patterns. However, Rb and Pb predominated in headwater moraines. In general, trace elements such as Co, Be, and Sb were more abundant in colluvium sites near metamorphic outcrops on both sides, and high levels of La were associated with moraines, while Cd and especially Mo contents were high in swamps and colluvium on the east side. Compared to the geochemical contents in the landforms, the streambed sediments were significantly enriched ($p \leq 0.05$) in ^{238}U, K, Na, Mg, As, Zn, Pb, Rb, Ni and La, but showed substantial depletion in ^{137}Cs and ^{210}Pb$_{ex}$, Mo and Sb.

In reference to the geochemical transfer from the proglacial area near the glacier tongue to the wetland shallow lake in the valley, distinct patterns were observed in the streambed sediments along the main stream draining the moraines at the headwaters and the wetlands in the glacial valley (Fig. 4). Fallout ^{137}Cs was only detected at the outlet of the expanding lake (S2) and the initial point of the wetlands (S3), with lower activity levels. However, ^{210}Pb$_{ex}$ activities increased at the headwaters and then decreased in the wetlands, mirroring the trend seen for ^{40}K. In contrast, radionuclide activities from the U and Th series, especially ^{238}U and ^{232}Th, increased in the wetlands.

Regarding the stable elements, important variations were observed in the streambed sediments (Fig. 5). Major elements (Fe, Al, Mg, Ca, Mn, and B) showed clear increment along the stream course. Minor elements (Li, Rb, Ni, and Co) and Cd contents exhibited slight increases. Conversely, substantial decreases were recorded in S, Pb, and Cu, while Cr content reduction was more moderate. Certain elements such as Si and Na, as well as P and Mo displayed relatively uniform distribution along the stream. However, no distinct patterns were evident for K, Ti, and V. Thallium showed significant variations, while La content exhibited less prominent variation. Additionally, Se and Sb were exclusively detected in the moraines near the glacier tongue.

3.2. Quantifying the contribution of the landforms to the streambed sediments

To identify the origin of sediments in the streambed samples collected at the final point within the wetland shallow lake (sediment mixture S5, Fig. 1) we used the latest version of the FingerPro R package. By applying the CR and CI methods (Table 4a) and selecting pairs with CTS (Table 4b), we identified the optimal pair of V and Ti to which the consensual tracers S, ^{232}Th, ^{40}K and Si were added, resulting in the

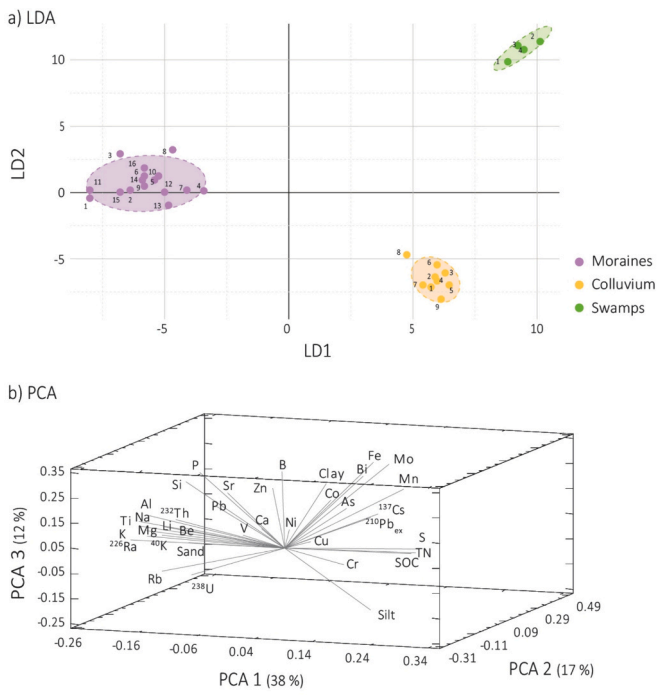

Fig. 3. a) 2D scatter plot diagram of the Linear Discrimination Analysis of the stable elements and radionuclides for the different landforms: moraines, colluvium and swamps. b) 3D scatter plot diagram of the Principal Component Analysis showing vectors of soil properties (Clay, Silt, Sand, SOC, TN), stable elements and radionuclides for the study landforms.

selected tracer set: V, Ti, S, ^{232}Th, ^{40}K and Si.

As depicted in the triangles of Fig. 6, out of the six chosen tracers V, Ti, S, ^{232}Th, ^{40}K and Si, V exhibited the highest values in colluvium, while S content was highest in swamps. Additionally, Ti, ^{232}Th, ^{40}K, and Si contents, that were the lowest in swamps, served as effective discriminators, proving to be optimal tracers for estimating the proportionate contribution of the study landforms. The density graph in Fig. 6 displayed well defined peaks and minimal dispersion.

The predominant contribution emerged from moraines, contributing as much as 54.2 ± 9.7 % of the sediment composition in the streambed mixture S5. Subsequently, colluvium materials contributed to a lower extent, around 39.2 ± 8.9 %, whereas swamps made the smallest contribution, accounting for <6.6 ± 2.4 %.

4. Discussion

Considering the origin of the landforms and the geomorphic processes involved, the grain size distribution was generally quite uniform. However, significant differences in the sand content of moraines (Table 1), suggest larger mineralogical components resulting from glacial processes compared to colluvium and swamps. The most significant differences were found in nutrient content. Soil organic carbon (SOC), active and stable carbon fractions, and Total Nitrogen (TN), exhibited their highest values in swamps, contrasting sharply with the other landforms (Table 1). The elevated soil nutrient content suggests very active soil processes and dynamic interplay between soil and plants in swamps, governed by the hydromorphic conditions associated with springs (Liberman, 2021). This contrasts with limited or negligible soil development observed in colluvium and recently exposed moraines. Consequently, pH and electrical conductivity levels are highest in swamps, buffering the acidic pH inherent in the glacial materials.

The abundance of major elements (Al, Fe, Si, K, Na, Ca, and Mg) aligns with the mineral composition of granite and granodiorite rocks found in the Huayna-Potosí batholite, which includes quartz, feldspars (microcline, plagioclases), and micas (Cordani et al., 2019). Similar major elements are also present in quartzites and schists of the Palaeozoic Amutara Formation. However, due to its sedimentary origin and subsequent transformation from contact metamorphism (Sempere et al., 2002), these formations exhibit lower contents of Al, Si, Na, Ca, and Mg. Therefore, the presence of these major elements indicates that silicates, particularly K feldspars and Na- and Al-rich plagioclases (Kabata-Pendias, 2011), form the main components of the fine silty matrix in the study landforms, which are primary fine sediment sources for the streambed deposits, aligning with their compositional characteristics (Table 2).

Nevertheless, the significant differences observed in swamps, particularly in comparison to moraines and colluvium, underscore the influence of soil processes driving the accumulation of various elements within the organic rich soil. Notably, elements such as Fe, S, and Mn, likely originated from Fe and Mn sulfides are associated with the hydromorphic and redox conditions found in swamps (Kabata-Pendias, 2011). Besides the existence of pyrite (Cordani et al., 2019; Sempere et al., 2002), the potential presence of Fe and Mn nodules in swamps soils cannot be discarded. In contrast, the depleted levels of Al, Si, K, Na, and other minor and trace elements are likely linked to the lower abundance of mineral material found in the organically enriched soils of the swamps (Table 1).

Furthermore, the depletion of elements like Ti, V, Cu, Rb, and Ni may be a consequence of their solubilization and subsequent export, facilitated by the prevalence of humic and fulvic substances (Stevenson, 1983). Conversely, the elevated levels of Tl and As could be attributed to specific S minerals such as lorandite (TlAsS2) and As-rich pyrite, or possibly due to sulfide oxidation (Kabata-Pendias, 2011). To a lesser degree, the slightly higher Cd content in swamps compared to moraines and colluvium may be attributed to its affinity for S (Kabata-Pendias, 2011), suggesting that the adsorption mechanism, enhanced by organic matter in swamps, could be relevant. The substantial organic matter content in swamps likely plays a major role in the recycling of geochemical elements, facilitating both solubilization of elements and retention through specific bonds (Tipping, 1981).

At the glacier tongue, the absence of ^{137}Cs indicates that the actual fresh moraines remained beneath ice cover during the period of ^{137}Cs fallout, with the peak fallout occurring in 1964–1965 in South America (Chaboche et al., 2021, 2022) and ending in 1980. The low levels of ^{210}Pb$_{ex}$, which experiences constant fallout, further support the idea that the area in close proximity to the glacier tongue was under ice cover and has only become exposed within the last four to five decades. Besides, the findings from the aerial survey conducted in 1975 by the Bolivian Air Force (FAB) and the analysis of high-resolution panchromatic images of 2021 from the Brazilian satellite CBERS-4 A (Fig. 1 Supplementary Material) also provide evidence of the retreat of the Huayna Potosí glacier. These outcomes highlight the swift pace of glacial recession and its environmental effects.

The presence of ^{137}Cs fallout has demonstrated its efficacy as a radiotracer (Evrard et al., 2020) and especially for tracking glacier retreat as it has been observed in other recently deglaciated regions of maritime Antarctica (Navas et al., 2017, 2018).

Conversely, the high levels of both fallout radionuclides within swamps highlight their strong association with organic matter and the efficiency of their binding mechanisms, particularly concerning ^{210}Pb$_{ex}$ (Gaspar et al., 2017). The presence of ^{137}Cs in colluvium, contrasts with findings around Parón Lake in the Cordillera Blanca, Perú (Navas et al., 2022), where more energetic runoff led to the removal of ^{137}Cs fixed in fine particles through erosion.

The scenario differs markedly for lithogenic radionuclides that are components of mineral lattices and consequently less prevalent in the organically rich swamps. In these areas, activities for ^{226}Ra, ^{232}Th, and ^{40}K are half that of moraines and colluvium. However, the abundance of ^{238}U is likely associated to the occurrence of Zr, as detailed in the Huayna-Potosí Mountain by Cordani et al. (2019), who reported

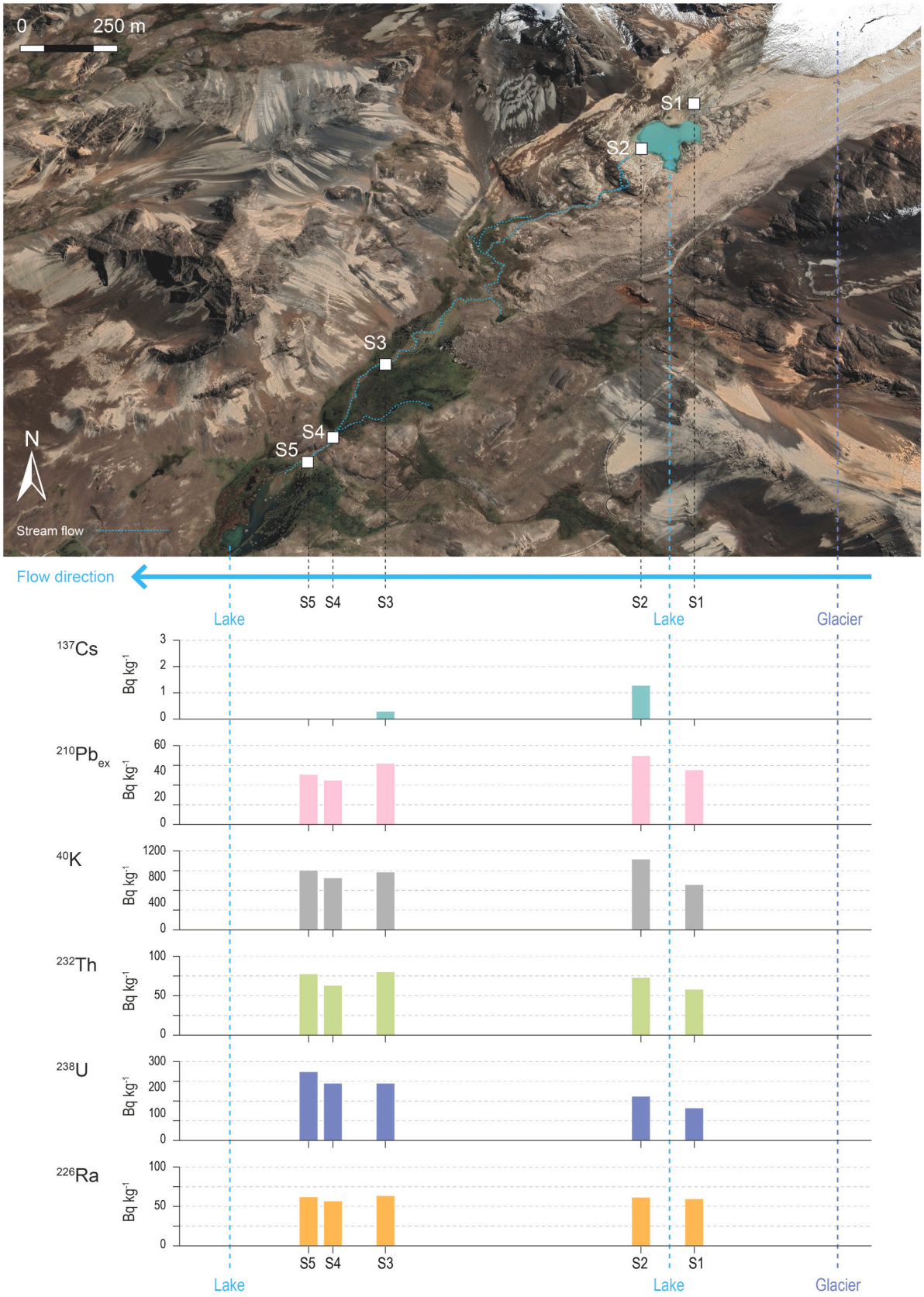

Fig. 4. Downstream variation of the fallout and lithogenic radionuclides mass activities in the streambed sediments collected in the proglacial area of Huayna-Potosí along the glacial valley from the glacier tongue (S1) to the wetland area ending in the ephemeral shallow lake (S5).

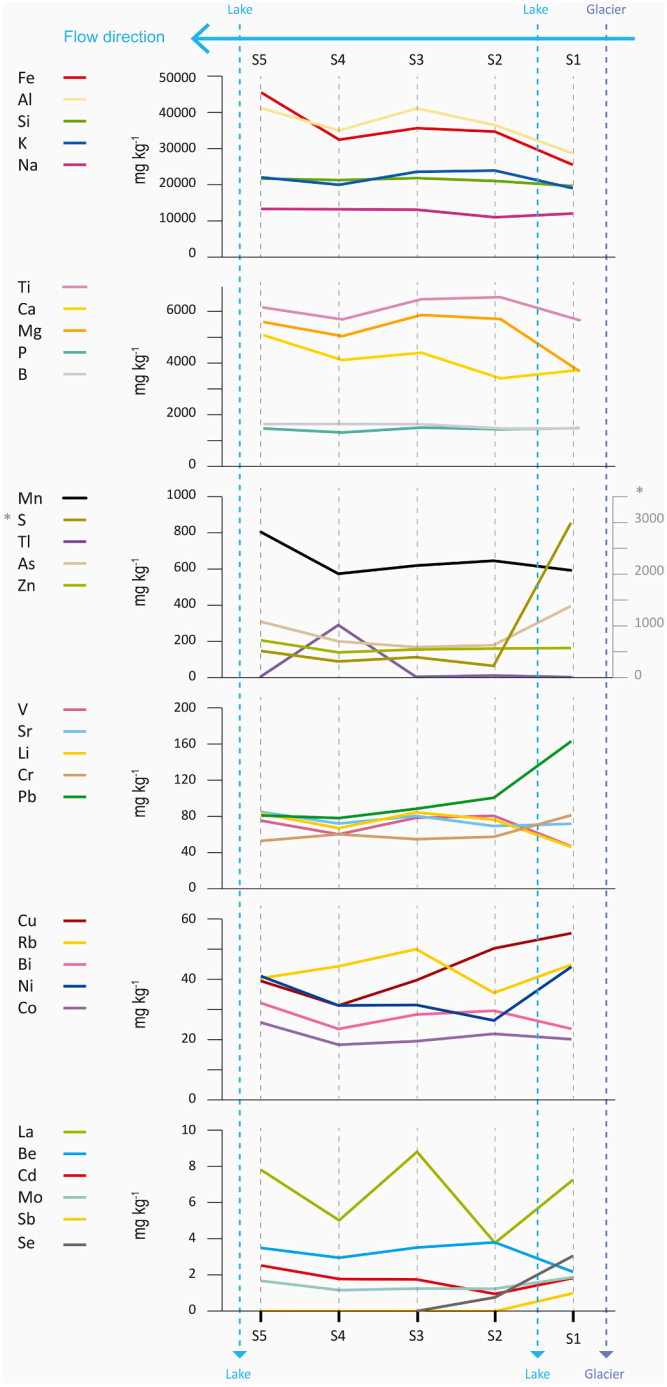

Fig. 5. Downstream variation of the stable elements content in the streambed sediments collected in the proglacial area of Huayna-Potosí along the glacial valley from the glacier tongue (S1) to the wetland area ending in the ephemeral shallow lake (S5).

exceptional uranium concentrations within zircon crystals.

The spatial distribution patterns of the geochemical levels clearly indicate the enrichment of ERNs and stable elements related to their abundance in igneous rocks and argillaceous materials. The high mineralization present in the rock outcrops along the eastern margin, associated with the contact metamorphism aureole, is likely the reason for the highest content of several stable elements in this area (Fig. 2 Supplementary Material). A different origin of high mineralization prevails in the same area, where the highest contents of S, Fe, and Mn in swamps indicate the abundance of sulfides, facilitated by the

Table 4
a) Values of consensus ranking (CR) and conservativeness index (CI) of the selected tracers and b) apportionments of the most discriminant pairs from the CTS analysis.

a)

Tracer	CR	CI %
V	97.4	51.36
S	97.4	44.64
Ti	96.8	45.40
^{232}Th	96.4	44.88
^{40}K	95.8	44.68
Si	93.7	44.94
Ca	90.9	45.42
^{226}Ra	86.9	46.72
^{214}Bi	75.4	45.20

b)

	Moraines		Colluvium		Swamps	
Tracer pairs	Mean	SD	Mean	SD	Mean	SD
V Ti	0.45	0.10	0.43	0.09	0.12	0.04
V ^{40}K	0.56	0.12	0.38	0.10	0.06	0.04
V S	0.55	0.13	0.38	0.10	0.06	0.05
V Si	0.60	0.15	0.36	0.10	0.04	0.08
V ^{232}Th	0.61	0.17	0.36	0.12	0.03	0.07

hydromorphic (Liberman, 2021) and redox conditions present in this sector. Additionally, the high content of a few elements such as Pb, Rb, and B, along with S, are governed by mineralogy of highly reactive moraines that have been recently exposed near the glacier tongue.

Within the domain of the recently exposed moraines, there is a general increase in radionuclide contents in streambed sediments at the outlet of the expanding lake. This increase is likely due to the accumulation of fine siliciclastic material containing both lithogenic and fallout radionuclides in the lake. Further down the valley, in the wetland domain, the disappearance of ^{137}Cs is observed in S3 (Fig. 4). Processes that could lead to depletion of FRNs include the selective export by runoff of finer and lighter organic material containing the fallout radionuclides, as well as the dilution effect following mixing in the streams with materials devoid of ^{137}Cs. Besides, both ^{137}Cs and ^{210}Pbex can be retained by the organic-rich soils of the wetlands due to their adsorption by organic matter (Gaspar et al., 2017; Martinez et al., 2010).

In contrast, the continuous increasing trend in ^{238}U content, and to a lesser extent in ^{232}Th, may reflect the accumulation of Th-bearing accessory minerals and U-rich Zr crystals, as reported by Cordani et al. (2019). However, in the case of ^{238}U, high mobility has been reported in various environments (Cowart and Burnett, 1994), as well as in other siliciclastic sedimentary substrates (Navas et al., 2002), in contrast to the low mobility of ^{232}Th (Navas et al., 2005).

The stable elements are transported through the main stream and small tributaries that drain the moraines at the headwater and wetland areas. The overall increase in certain elements displays variations ranging from substantial increments in major elements (e.g. Fe, Al, Ca, Mn) to more modest changes (e.g. Co, Cd). This indicates a trend towards a geochemical particulate transfer linked to fine particles, which involves up to 10 elements. However, Si, B, P and Na exhibit relative uniformity along the stream course, suggesting their stabilization within the fine material of the streambed or may be attributed to the absence of additional significant sources of input or export for these elements.

Conversely, significant reductions in Pb, Cu, and to a lesser extent Cr and Sb, suggest their retention within the rich organic soils of wetlands covered by dense vegetation, which includes both flattened and protruding cushions. These soils experience water saturation conditions (Liberman, 2021). Although water stored in these cushions flows gradually, it is worth noting that even during the dry season when continuous water delivery occurred during the field sampling, the running

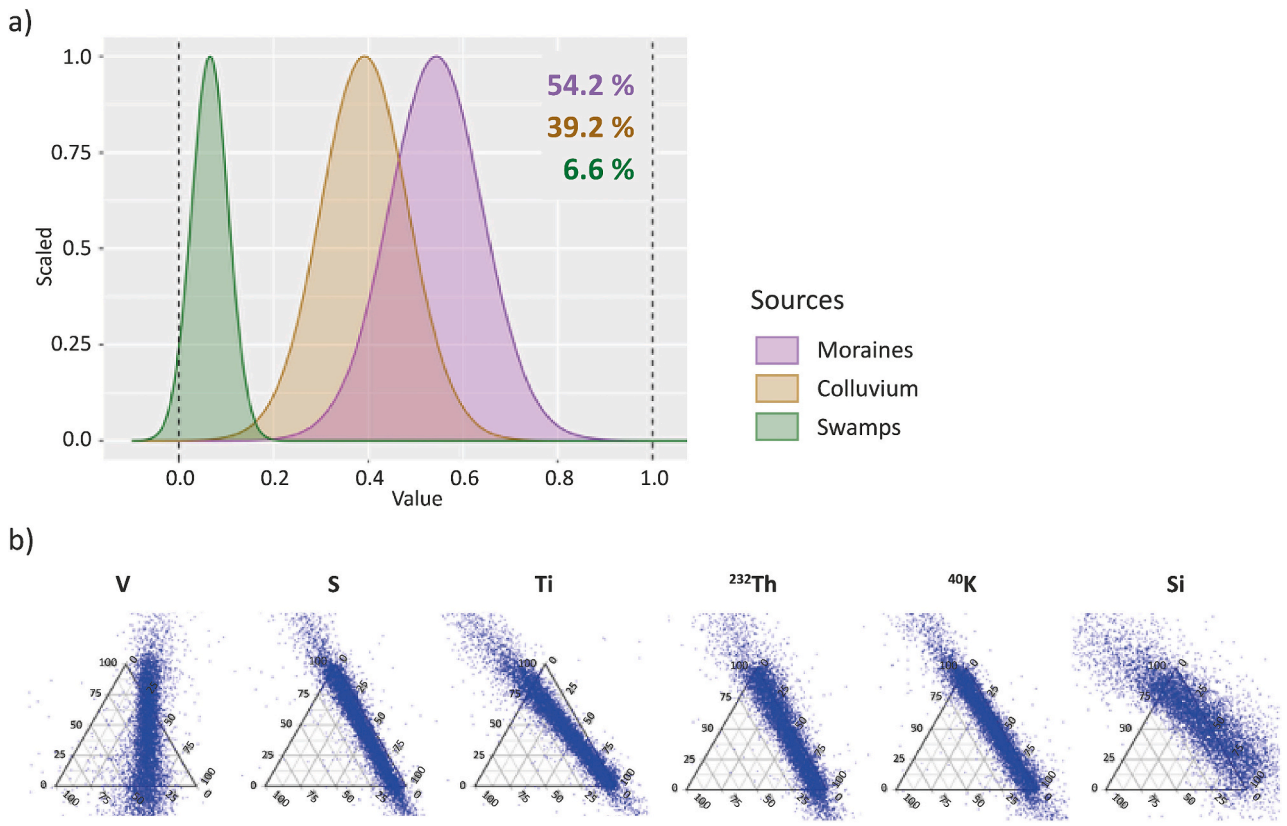

Fig. 6. Percentage contribution from the three landforms, obtained with the consistency method (CTS), to the sediment mixture S5, located in the ephemeral shallow lake of the wetland area. a) Density graph of the unmixing results from FingerPro model and b) ternary diagrams of the tracers selected by applying CI and CR methods.

water appeared clear and devoid of any particulate matter. This emphasizes the effective role of wetland vegetation in capturing sediments, as well as certain associated elements and nutrients. This phenomenon highlights the crucial function of vegetation in water filtration, ultimately leading to a reduction in sediment load (Buytaert et al., 2011).

The geological setting of the study area comprises Quaternary formations, including moraines and colluvium mantles. Colluvium deposits rest atop high-gradient slopes at the base of Palaeozoic reliefs, originating from intense periglacial processes. These landforms overlay the underlying rock substrate. Cryoclastic processes, freeze-thaw cycles, rock failures, snow avalanches, debris flows, and glacial erosion collectively contribute to the weathering of the underlying rocks within the proglacial area. As a result, the materials of these landforms disintegrate into fine particles, which are then transported by runoff within a complex cascade of sediment fluxes.

Concerning the identification of sediment provenance, among the conservative and consensual tracers ^{232}Th and ^{40}K activities, along with Si, are influenced by prevalent siliciclastic components in moraines and colluvium. Their elevated activities in streambed sediments of S5 mixture further emphasize their bond with argillaceous minerals, linked to the abundance of clay and silt sizes in S5. Ti, a significant component in silicates (Kabata-Pendias, 2011), explains its prevalence in moraines and colluvium. In contrast, S content is six to eight times higher in swamps, while V, present in argillaceous sedimentary rocks and also originating from secondary sources (Kabata-Pendias, 2011), exhibits its highest levels in colluvium.

The extensive coverage of moraines resulting from various glacier retreat periods post the Little Ice Age (LIA), coupled with their high connectivity, leads to significant sediment delivery from this source. Consequently, moraines contribute up to 54 % of the sediment in the S5 streambed mixture within the shallow wetland lake (Fig. 6). Moreover, the direct connectivity and steep slopes of colluvium mantles also play a significant role, accounting for 39 % of the sediment contribution. This pattern aligns with findings from the tropical highlands of the Artesonraju Glacier in the Peruvian Cordillera Blanca, where Navas et al. (2022) observed that moraines were the primary sediment source for fine sediment.

The principal contributions from both landforms stem from their scarce vegetation coverage, making the exposed surfaces of moraines and colluvium highly reactive. As a result, runoff and snowmelt over these sparsely vegetated landforms contribute significantly (93 %) to the supply of fine sediment that rapidly reaches the streams.

The recently exposed moraines near the glacier tongue, devoid of vegetation, are likely to supply substantial amounts of sediment during ice melt. The steepness colluvium deposits promotes intense slope/gravitational and runoff processes, hindering soil development compared to the more developed soils found in slope swamps and valley floor's wetlands, which explains their relatively high sediment contribution.

In contrast, the stability of swamps, protected by a dense covering of cushions and aquatic macrophytes, effectively limits erosion. Furthermore, the retention of sediment and particle aggregation, facilitated by the abundant organic matter, greatly reduces their sediment contribution to <7 %. This is remarkable considering the steep slopes and intricate network of small streams that continually incise and drain their surfaces, suggesting the effectiveness of swamps in sediment retention and erosion control.

It is important to note that sampling was conducted during the dry season, with no precipitation before or during the campaign. Consequently, no runoff was observed on the landforms, and runoff from ice melt and swamps carried insignificant sediment load (mean suspended sediment concentration of 8 samples collected from streams during the

campaign was 42.7 ± 2.6 mg/|L). However, it is worth considering that different conditions could arise during wet periods or heavy rainfall events. In such situations, contributions from these landforms may vary, as observed in temperate environments following exceptional precipitation events (Gaspar et al., 2019b).

Furthermore, research conducted in other proglacial areas has shown that stronger floods during snowmelt (Navas et al., 2020) and intense rainfall events (Navas et al., 2022) can lead to intensified erosion, particularly during the peak of the melting season or El Niño events. This has been confirmed by on-site flood observations after rainfall events in the Huayna-Potosí area, where substantial sediment flux into streams was observed.

5. Conclusions

This study underlines the distinctive geochemical compositions of the study landforms, which arise from their lithological characteristics and formation processes. Moraines, are intricately tied to glacier processes and retreat, while for colluvium, the central operational processes encompass freeze-thaw cycles and gravity. In contrast, swamps are formed under hydromorphic conditions, leading to the accumulation of organic matter and distinctive compositions with the highest levels of nutrients, fallout radionuclides and elements such as S, Fe, and Mn, besides Tl and As. This particularity arises not only from specific dissolution and fixation processes by the organic components but also due to lower content of siliciclastic materials. Moreover, the capacity of swamps to retain fine sediment serves to mitigate harmful impacts on water bodies.

The transfer of geochemical elements varied significantly along the stream course from the moraine domain at the headwater to the wetlands on the valley floor. At the final sampling point (S5 sediment mixture) in the wetland shallow lake, streambed sediments were enriched in ^{238}U and, to a lesser extent, in ^{232}Th, but depleted in other radionuclides. Additionally, there were substantial increases in major elements (Fe, Al, Mg, Ca and Mn), significant decreases in Pb and Cu, and moderate depletions for Cr and Sb. The complex interplay of processes within both the glacial-periglacial and wetland domains underlies the observed compositional variations along the stream with adsorption, solubilization, and retention within the wetlands governing biogeochemical cycles and element distribution. Therefore, preserving high-altitude wetlands as buffers for recently exposed areas is essential.

The intense physical weathering across moraines and colluvium drives the highest sediment delivery in the proglacial area, likely enhanced by high water levels during snow and ice melting and wet seasons, especially during El Niño events. Further research into sediment and geochemical dynamics linked to glacier shrinkage, especially during high water levels, is required. Monitoring sediment influx from moraines and colluvium is crucial for sediment control, preventing the infilling of lakes and regulated dams. Given glacier decline, the preservation of high altitude wetlands is vital for water supply to La Paz and El Alto cities, as well as for supporting ecosystems and the regional economy.

Supplementary data to this article can be found online at https://doi.org/10.1016/j.geomorph.2024.109250.

CRediT authorship contribution statement

Ana Navas: Writing – original draft, Resources, Project administration, Methodology, Investigation, Funding acquisition, Formal analysis, Conceptualization. **Edson Ramírez:** Writing – review & editing, Resources, Project administration, Investigation. **Leticia Gaspar:** Writing – review & editing, Validation, Methodology, Investigation, Formal analysis, Data curation. **Ivan Lizaga:** Writing – review & editing, Software, Methodology, Investigation, Formal analysis, Data curation. **Tim Stott:** Writing – review & editing, Resources, Investigation. **Francisco Rojas:** Writing – review & editing, Investigation, Data curation. **Borja Latorre:** Writing – review & editing, Software, Methodology, Investigation, Formal analysis, Data curation. **Gerd Dercon:** Writing – review & editing, Resources, Project administration, Investigation, Conceptualization.

Declaration of competing interest

The authors declare that they have no known competing financial interests or personal relationships that could have appeared to influence the work reported in this paper.

Data availability

Data will be made available on request.

Acknowledgements

This research was financially supported by the IAEA Interregional Technical Cooperation Project INT5153 “Assessing the Impact of Climate Change and its Effects on Soil and Water Resources in Polar and Mountainous Regions” funded by IAEA and by project PID2019-104857RB-I00 funded by the Spanish National Research Agency. We gratefully acknowledge to all participants in the 2017 IAEA mission, especially to Michele Nuñez, Rubén Callisaya, Iris Calle, Bulat Mavlyudov and Osama Mustafa.

References

Abott, M.B., Wolfe, B.B., Aravena, R., Wolfe, A.P., Seltzer, G.O., 2000. Holocene hydrological reconstruction from stable isotopes and paleoclimatology. Cordillera Real, Bolivia. Quat. Sci. Rev. 19, 1801–1820.

Baraer, M., Mark, B.G., McKenzie, J.M., Condom, T., Bury, J., Huh, K., Portocarrero, C., Gómez, J., Rathay, S., 2012. Glacier recession and water resources in Peru's Cordillera Blanca. J. Glaciol. 58, 134–150. https://doi.org/10.3189/2012JoG11J186.

Blake, W.H., Boeckx, P., Stock, B.C., Smith, H.G., Bodé, S., Upadhayay, H.R., Gaspar, L., Goddard, R., Lennard, A.T., Lizaga, I., Lobb, D.A., Owens, P.N., Petticrew, E.L., Kuzyk, Z.Z.A., Gari, B.D., Munishi, L., Mtei, K., Nebiyu, A., Mabit, L., Navas, A., Semmens, B.X., 2018. A deconvolutional Bayesian mixing model approach for river basin sediment source apportionment. Sci. Rep. 8, 13073 https://doi.org/10.1038/s41598-018-30905-9.

Bradley, R.S., Vuille, M., Diaz, H.F., Vergara, W., 2006. Threats to water supplies in the Tropical Andes. Science 312, 1755–1756. https://doi.org/10.1126/science.1128087.

Buytaert, W., Vuille, M., DeWulf, A., Urrutia, R., Karmalkar, A., Celleri, R., 2010. Uncertainties in climate change projections and regional downscaling in the tropical Andes: implications for water resources management. Hydrol. Earth Syst. Sci. 14, 1247–1258. https://doi.org/10.5194/hess-14-1247-2010.

Buytaert, W., Cuesta-Camacho, F., Tobón, C., 2011. Potential impacts of climate change on the environmental services of humid tropical alpine regions. Glob. Ecol. Biogeogr. 20, 19–33. https://doi.org/10.1111/j.1466-8238.2010.00585.x.

Chaboche, P.-A., Saby, N.P.A., Laceby, J.P., Minella, J.P.G., Tiecher, T., Ramon, R., Tassano, M., Cabral, P., Cabrera, M., da Silva, Y.J.A.B., Lefevre, I., Evrard, O., 2021. Mapping the spatial distribution of global ^{137}Cs fallout in soils of South America as a baseline for Earth Science studies. Earth Sci. Rev. 214, 103542 https://doi.org/10.1016/j.earscirev.2021.103542.

Chaboche, P.-A., Pointurier, F., Sabatier, P., Foucher, A., Tiecher, T., Minella, J.P.G., Tassano, M., Hubert, A., Morera, S., Guédron, S., Ardois, C., Boulet, B., Cossonnet, C., Cabral, P., Cabrera, M., Chalar, G., Evrard, O., 2022. ^{240}Pu/^{239}Pu signatures allow refining the chronology of radionuclide fallout in South America. Sci. Total Environ. 843, 156943 https://doi.org/10.1016/j.scitotenv.2022.156943.

Collins, A.L., Walling, D.E., 2002. Selecting fingerprint properties for discriminating potential suspended sediment sources in river basins. J. Hydrol. 261, 218–244. https://doi.org/10.1016/S0022-1694(02)00011-2.

Collins, A.L., Blackwell, M., Boeckx, P., Chivers, C.-A., Emelko, M., Evrard, O., Foster, I., Gellis, A., Gholami, H., Granger, S., Harris, P., Horowitz, A.J., Laceby, J.P., Martinez-Carreras, N., Minella, J., Mol, L., Nosrati, K., Pulley, S., Silins, U., da Silva, Y.J.A.B., Stone, M., Tiecher, T., Upadhayay, H.R., Zhang, Y., 2020. Sediment source fingerprinting: benchmarking recent outputs, remaining challenges and emerging themes. J. Soils Sediments 20, 4160–4193. https://doi.org/10.1007/s11368-020-02755-4.

Cordani, U.G., Iriarte, A.R., Sato, K., 2019. Geochronological systematics of the Huayna Potosí, Zongo and Taquesi plutons, Cordillera real of Bolivia, by the K/Ar, Rb/Sr and U/Pb methods. Braz. J. Geol. 49, 1–22. https://doi.org/10.1590/2317-4889201920190016.

Cowart, J.B., Burnett, W.C., 1994. The distribution of uranium and thorium decay- series radionuclides in the environment. J. Environ. Qual. 23, 651–662. https://doi.org/10.2134/jeq1994.00472425002300040005x.
Dangles, O., Rabatel, A., Kraemer, M., Zeballos, G., Soruco, A., Jacobsen, D., Anthelme, F., 2017. Ecosystem sentinels for climate change? Evidence of wetland cover changes over the last 30 years in the tropical Andes. PLoS One 12 (5), e0175814. https://doi.org/10.1371/journal.pone.0175814.
Evrard, O., Chaboche, P.-A., Ramon, R., Foucher, A., Laceby, J.P., 2020. A global review of sediment source fingerprinting research incorporating fallout radiocesium (^{137}Cs). Geomorphology 362, 107103. https://doi.org/10.1016/j.geomorph.2020.107103.
Fraser, B., 2012. Melting in the Andes: Goodbay glaciers. Nature 491, 180–182. https://doi.org/10.1038/491180a.
Garreaud, R., Vuille, M., Clement, A., 2003. The climate of the Altiplano: observed current conditions and mechanisms of past changes. Palaeogeogr. Palaeoclimatol. Palaeoecol. 194, 5–22. https://doi.org/10.1016/S0031-0182(03)00269-4.
Gaspar, L., Webster, R., Navas, A., 2017. Fate of $^{210}Pb_{ex}$ fallout in soil under forest and scrub of the central Spanish Pre-Pyrenees. Eur. J. Soil Sci. 68, 259–269. https://doi.org/10.1111/ejss.12427.
Gaspar, L., Blake, W.H., Smith, H.G., Lizaga, I., Navas, A., 2019a. Testing the sensitivity of a multivariate mixing model using geochemical fingerprints with artificial mixtures. Geoderma 337, 498–510. https://doi.org/10.1016/j.geoderma.2018.10.005.
Gaspar, L., Lizaga, I., Blake, W.H., Latorre, B., Quijano, L., Navas, A., 2019b. Fingerprinting changes in source contribution for evaluating soil response during an exceptional rainfall in Spanish Pre-Pyrenees. J. Environ. Manag. 240, 136–148. https://doi.org/10.1016/j.jenvman.2019.03.109.
Kabata-Pendias, A., 2011. Trace Elements in Soils and Plants, fourth ed. CRC Press, Boca Raton. https://doi.org/10.1201/b10158.
Knight, J., Harrison, S., 2018. Transience in cascading paraglacial systems. Land Degrad. Dev. 29, 1991–2001. https://doi.org/10.1002/ldr.2994.
Latorre, B., Lizaga, I., Gaspar, L., Navas, A., 2021. A novel method for analysing consistency and unravelling multiple solutions in sediment fingerprinting. Sci. Total Environ. 789, 147804 https://doi.org/10.1016/j.scitotenv.2021.147804.
Li, D., Xixi, L., Overeem, I., Walling, D.E., Syvitski, J., Kettner, A.J., Bookhagen, B., Zhou, Y., Zhang, T., 2021. Exceptional increases in fluvial sediment fluxes in a warmer and wetter High Mountain Asia. Science 374, 599–603. https://doi.org/10.1126/science.abi9649.
Liberman, M., 2021. Climate change, wetland management and alpaca pastoralism in the Bolivian high Andes mountains. In: Pedrotti, F., Box, E.O. (Eds.), Tools for Landscape-Scale Geobotany and Conservation. Geobotany Studies. Springer, Cham, pp. 65–98. https://doi.org/10.1007/978-3-030-74950-7_5.
Lizaga, I., Latorre, B., Gaspar, L., Navas, A., 2020a. FingerPro: an R package for tracking the provenance of sediment. Water Resour. Manag. 34, 3879–3894. https://doi.org/10.1007/s11269-020-02650-0.
Lizaga, I., Latorre, B., Gaspar, L., Navas, A., 2020b. Consensus ranking as a method to identify non-conservative and dissenting tracers in fingerprinting studies. Sci. Total Environ. 720, 137537 https://doi.org/10.1016/j.scitotenv.2020.137537.
Lizaga, I., Latorre, B., Bodé, S., Gaspar, L., Boeckx, P., Navas, A., 2024. Combining isotopic and elemental tracers for enhanced sediment source partitioning in complex catchments. J. Hydrol. 631, 130768 https://doi.org/10.1016/j.jhydrol.2024.130768.
Llambí, L.D., Cuesta, F., 2014. La diversidad de los páramos andinos en el espacio y en el tiempo. In: Cuesta, F., Sevink, J., Llambí, L.D., De Bièvre, B., Posner, J. (Eds.), Avances en Investigación para la Conservación de los Páramos Andinos. CONDESAN. Universidad de Amsterdam, ICAE-Universidad de Los Andes, Universidad de Wisconsin, Lima, pp. 8–38.
López Alba, F., 2014. Fotogrametría terrestre aplicada a investigaciones glaciológicas (caso glaciar Charquini Sur, 16°S). Universidad Mayor de San Andrés, La Paz, Bolivia, Tesis de Grado. https://repositorio.umsa.bo/xmlui/handle/123456789/20004.
Lopez-Moreno, J.I., Motran-Tejeda, E., Vicente-Serrano, S.M., Bazo, J., Azorin-Molina, C., Revuelto, J., Sanchez-Lorenzo, A., Navarro-Serrano, F., Aguilar, E., Chura, O., 2016. Recent temperature variability and change in the Altiplano of Bolivia and Peru. Int. J. Climatol. 36, 1773–1796. https://doi.org/10.1002/joc.4459.
Loza Herrera, S., Meneses, R.I., Anthelme, F., 2015. Plant communities of high-Andean wetlands of the Cordillera real (Bolivia) in the face of global warming. Ecol. Bolivia 50 (1), 39–56.
Martinez, C., Hancock, G.R., Kalma, J.D., 2010. Relationships between ^{137}Cs and soil organic carbon (SOC) in cultivated and never-cultivated soils, an Australian example. Geoderma 158, 137–147. https://doi.org/10.1016/j.geoderma.2010.04.019.
Martínez-Carreras, N., Krein, A., Gallart, F., Iffly, J.F., Pfister, L., Hoffmann, L., Owens, P. N., 2010. Assessment of different colour parameters for discriminating potential suspended sediment sources and provenance: a multi-scale study in Luxembourg. Geomorphology 118, 118–129. https://doi.org/10.1016/j.geomorph.2009.12.013.
Navas, A., Machín, J., 2002. Spatial distribution of heavy metals and arsenic in soils of Aragón (NE Spain): controlling factors and environmental implications. Appl. Geochem. 17, 961–973. https://doi.org/10.1016/S0883-2927(02)00006-9.
Navas, A., Soto, J., Machín, J., 2002. ^{238}U, ^{226}Ra, ^{210}Pb, ^{232}Th and ^{40}K activities in soil profiles of the Flysch sector (Central Spanish Pyrenees). Appl. Radiat. Isot. 57 (4), 579–589. https://doi.org/10.1016/S0969-8043(02)00131-8.
Navas, A., Soto, J., Machín, J., 2005. Mobility of natural radionuclides and selected major and trace elements along a soil toposequence in the central Spanish Pyrenees. Soil Sci. 170 (9), 743–757. https://doi.org/10.1097/01.ss.0000185906.18460.65.
Navas, A., Oliva, M., Fernández, J., Gaspar, L., Quijano, L., Lizaga, I., 2017. Radionuclides and soil properties as indicators of glacier retreat in a recently deglaciated permafrost environment of the Maritime Antarctica. Sci. Total Environ. 609, 192–204. https://doi.org/10.1016/j.scitotenv.2017.07.115.
Navas, A., Serrano, E., López-Martínez, J., Gaspar, L., Lizaga, I., 2018. Interpreting environmental changes from radionuclides and soil characteristics in different landform contexts of Elephant Island (Maritime Antarctica). Land Degrad. Dev. 29, 3141–3158. https://doi.org/10.1002/ldr.2987.
Navas, A., Lizaga, I., Gaspar, L., Latorre, B., Dercon, G., 2020. Unveiling the provenance of sediments in the moraine complex of Aldegonda Glacier (Svalbard) after glacial retreat using radionuclides and elemental fingerprints. Geomorphology 367, 107304. https://doi.org/10.1016/j.geomorph.2020.107304.
Navas, A., Lizaga, I., Santillán, N., Gaspar, L., Latorre, B., Dercon, G., 2022. Targeting the source of fine sediment and associated geochemical elements by using novel fingerprinting methods in proglacial tropical highlands. (Cordillera Blanca, Perú). Hydrol. Process. 36, e14662 https://doi.org/10.1002/hyp.14662.
Owens, P.N., Blake, W.H., Gaspar, L., Gateuille, D., Koiter, A.J., Lobb, D.A., Petticrew, E. L., Reiffarth, D.G., Smith, H.G., Woodward, J.C., 2016. Fingerprinting and tracing the sources of soils and sediments: Earth and ocean science, geoarchaeological, forensic, and human health applications. Earth Sci. Rev. 162, 1–23. https://doi.org/10.1016/j.earscirev.2016.08.012.
Quijano, L., Gaspar, L., Navas, A., 2016. Lateral and depth patterns of soil organic carbon fractions in a mountain Mediterranean agrosystem. J. Agric. Sci. 154 (2), 287–304. https://doi.org/10.1017/S002185961400135X.
da R Ribeiro, R., Ramirez, E., Simões, J.C., Machaca, A., 2013. 46 years of environmental records from the Nevado Illimani glacier group, Bolivia, using digital photogrammetry. Ann. Glaciol. 54 (63) https://doi.org/10.3189/2013AoG63A494.
da R Ribeiro, R., Simões, J.C., Ramirez, E., 2017. The Amazon Glaciers. In: Glaciers Evolution in a Changing World. Intech. https://doi.org/10.5772/intechopen.70490.
Rabatel, A., Francou, B., Jomelli, V., Naveau, P., Grancher, D., 2008. A chronology of the Little Ice Age in the tropical Andes of Bolivia (16 S) and its implications for climate reconstruction. Quat. Res. 70, 198–212. https://doi.org/10.1016/j.yqres.2008.02.012.
Rabatel, A., Francou, B., Soruco, A., Gomez, J., Cáceres, B., Ceballos, J.L., Basantes, R., Vuille, M., Sicart, J.-E., Huggel, C., Scheel, M., Lejeune, Y., Arnaud, Y., Collet, M., Condom, T., Consoli, G., Favier, V., Jomelli, V., Galarraga, R., Ginot, P., Maisincho, L., Mendoza, J., Ménégoz, M., Ramirez, E., Ribstein, P., Suarez, W., Villacis, M., Wagnon, P., 2013. Current state of glaciers in the tropical Andes: a multi-century perspective on glacier evolution and climate change. Cryosphere 7, 81–102. https://doi.org/10.5194/tc-7-81-2013.
Ramírez, E., Francou, B., Ribstein, P., Descloitres, M., Guérin, R., Mendoza, J., Gallaire, R., Pouyaud, B., Ekkehard, J., 2001. Small glaciers disappearing in the tropical Andes: a case-study in Bolivia: Glaciar Chaclataya (16° S). J. Glaciol. 47, 187–194. https://doi.org/10.3189/172756501781832214.
Réveillet, M., Rabatel, A., Gillet-Chaulet, F., Soruco, A., 2015. Simulations of changes to Glaciar Zongo, Bolivia (16° S), over the 21st century using a 3-D full-Stokes model and CMIP5 climate projections. Ann. Glaciol. 56, 89–97. https://doi.org/10.3189/2015AoG70A113.
Sempere, T., Carlier, G., Soler, P., Fornari, M., Carlotto, V., Jacay, J., Arispe, O., Néraudeau, D., Cárdenas, J., Rosas, S., Jiménez, N., 2002. Late Permian-Middle Jurassic lithospheric thinning in Peru and Bolivia, and its bearing on Andean-age tectonics. Tectonophysics 345, 153–181. https://doi.org/10.1016/S0040-1951(01)00211-6.
Soruco, A., Vincent, C., Rabatel, A., Francou, B., Thibert, E., Sicart, J.E., Condom, T., 2015. Impacts of glacier shrinkage on water resources of La Paz city, Bolivia (16°S). Ann. Glaciol. 56, 147–154. https://doi.org/10.3189/2015AoG70A001.
Stevenson, F.J., 1983. Trace metal-organic interactions in geologic environments. In: Augustithis, S.S., Minatidis, D.G. (Eds.), The Significance of Trace Elements in Solving Petrogenic Problems. Theophrastus Publications, Athens, pp. 671–691.
Strzelecki, M.C., Long, A.J., Lloyd, J.M., 2017. Post-Little Ice Age development of a high Arctic paraglacial beach complex. Permafr. Periglac. Process. 28, 4–17. https://doi.org/10.1002/ppp.1879.
Thompson, L.G., Davis, M.E., Mosley-Thompson, E., Sowers, T.A., Henderson, K.A., Zagorodnov, V.S., Lin, P.N., Mikhalenko, V.N., Campen, R.K., Bolzan, J.F., Cole-Dai, J., Fracou, B., 1998. A 25.000-year tropical climate history from Bolivian ice cores. Science 282, 1858–1864. https://doi.org/10.1126/science.282.5395.1858.
Tipping, E., 1981. The adsorption of aquatic humic substances by iron oxides. Geochim. Cosmochim. Acta 45, 191–199. https://doi.org/10.1016/0016-7037(81)90162-9.
Vuille, M., Bradley, R.S., Werner, M., Keimig, F., 2003. 20th century climate change in the tropical Andes: observations and model results. Clim. Chang. 59, 75–99. https://doi.org/10.1023/A:1024406427519.
Vuille, M., Francou, B., Wagnon, P., Juen, I., Kaser, G., Mark, B.G., Bradley, R.S., 2008. Climate change and tropical Andean glaciers: past, present and future. Earth Sci. Rev. 89, 79–96. https://doi.org/10.1016/j.earscirev.2008.04.002.
Vuille, M., Carey, M., Huggel, C., Buytaert, W., Rabatel, A., Jacobsen, D., Soruco, A., Villacis, M., Yarleque, C., Timm, O.E., Condom, T., Salzmann, N., Sicart, J.-E., 2018. Rapid decline of snow and ice in the tropical Andes – Impacts, uncertainties and challenges ahead. Earth Sci. Rev. 176, 195–213. https://doi.org/10.1016/j.earscirev.2017.09.019.